JOURNAL OF GEOPHYSICAL RESEARCH, VOL. 105, NO. B3, PAGES 6069–6088, MARCH 10, 2000

Influence of friction and fault geometry on earthquake rupture

Stefan B. Nielsen[1]
Institute of Crustal Studies, University of California, Santa Barbara

J. M. Carlson
Department of Physics, University of California, Santa Barbara

Kim B. Olsen
Institute of Crustal Studies, University of California, Santa Barbara

Abstract. We investigate the impact of variations in the friction and geometry on models of fault dynamics. We focus primarily on a three-dimensional continuum model with scalar displacements. Slip occurs on an embedded two-dimensional planar interface. Friction is characterized by a two-parameter rate and state law, incorporating a characteristic length for weakening, a characteristic time for healing, and a velocity-weakening steady state. As the friction parameters are varied, there is a crossover from narrow, self-healing slip pulses to crack-like solutions that heal in response to edge effects. For repeated ruptures the crack-like regime exhibits periodic or aperiodic systemwide events. The self-healing regime exhibits dynamical complexity and a broad distribution of rupture areas. The behavior can also change from periodicity or quasi-periodicity to dynamical complexity as the total fault size or the length-to-width ratio is increased. Our results for the continuum model agree qualitatively with analogous results obtained for a one-dimensional Burridge–Knopoff model in which radiation effects are approximated by viscous dissipation.

1. Introduction

In recent years, two issues have been the focus of a great deal of debate in the earthquake modeling community. The first is related to the dynamics of individual ruptures. Here the key question is whether the propagation of slip takes place in the form of an expanding crack or, alternatively, as a narrow, self-healing pulse. The second is related to the origin of complexity in the seismic cycle. Here the central issue is whether the observed broad distribution of sizes of events and irregular recurrence intervals can be attributed to frictional instabilities inherent in the dynamical equations of motion or whether fixed geometric irregularities are responsible. In this paper we explore these issues in the context of a three-dimensional continuum model and a one-dimensional Burridge–Knopoff model. In our studies, dynamical complexity refers to observations of a broad distribution in the rupture area, moment release, and recurrence interval associated with the large propagating ruptures and does not refer to any particular property at the small end of the spectrum. We observe that complexity and narrow rupture pulses are closely coupled and depend on friction properties and fault geometry.

Narrow slip-pulse solutions were first postulated by *Brune* [1970], who suggested that active slip might be restricted to a narrow, propagating band during an earthquake if the friction increased on the fault shortly after rupture. *Heaton* [1990] noted that a short rise time for the slip was compatible with observations for several earthquakes. In many continuum dynamical models, rate weakening friction appears to be an important ingredient for narrow pulse solutions. Indeed, crack-like ruptures have been widely observed in simulations with rate-independent friction laws [*Madariaga*, 1976; *Andrews*, 1976; *Day*, 1982; *Harris and Day*, 1993]. Pulse-like behavior has been observed in several simulations when rate weakening was included either in the form of a purely velocity-dependent friction law, a piecewise continuous friction with slip and velocity dependence, or a rate and state law with steady state velocity weakening [*Cochard and Madariaga*, 1994, 1996; *Perrin et*

[1]Also at Materials Research Lab, University of California, Santa Barbara.

Paper number 1999JB900350.
0148-0227/00/1999JB900350$09.00

al., 1995; *Beeler and Tullis*, 1996]. Recently, in the context of a rate and state friction law which included rate weakening, *Zheng and Rice* [1998] discussed the transition from crack-like to pulse-like rupture as a function of decreasing prestress. While we focus primarily on rate-weakening as the cause for the onset of premature healing, we emphasize that at least one other mechanism is known to induce relatively narrow rupture pulses. Indeed, in the presence of strong prestress heterogeneities, rupture models have led to the propagation of relatively narrow patches of active rupture [*Day et al.*, 1998; *Beroza and Mikumo*, 1996].

Many examples of complex spatial patterns and broad distributions of small and large events have been observed in lower-dimensional models and simplified representations, such as Burridge-Knopoff models [*Burridge and Knopoff*, 1967; *Carlson and Langer*, 1989a, b; *Carlson, et al.*, 1991, 1994] and cellular automata (see, e.g., *Christensen and Olami* [1992], *Chen, et al.* [1991], *Pepke, et al.* [1994], *Leung, et al.* [1998] and *Rundle, et al.* [1995]). In these systems, dynamical complexity seems to be the rule rather than the exception. Simulations of large system sizes and long time series lead to complex catalogs of events which can be used to study a variety of seismic phenomena, including scaling relations, correlations, and prediction.

For continuum models (i.e., models for which the Earth's crust is modeled as a continuous medium), evidence for dynamical complexity has been restricted to a comparatively narrow range of models and parameters. Instead, for continuum models, periodic or quasiperiodic behavior is more commonly observed. *Nielsen et al.* [1995] modeled a two-dimensional antiplane fault with time-dependent frictional weakening and obtained periodic solutions when the process zone of frictional decay at the fracture tip was expanded to a significant portion of the total length of the fault. For smaller process zones, periodicity was not observed. However, they still did not observe broad distributions of events. An example of a continuum model which does exhibit dynamical complexity was obtained by *Langer et al.* [1996]. They observed dynamical complexity in a two-dimensional Klein-Gordon model of the crustal plane. Here the third dimension is modeled by a leaf spring, so it has been referred to as a two-dimensional Burridge–Knopoff model. Additionally, *Cochard and Madariaga* [1994] modeled the continuum in three dimensions using the boundary integral method for a friction law which combined slip and rate weakening. In their studies, complexity did not arise from a purely slip weakening friction law. However, when the friction was modified to include rate weakening during the later stages of slip, they observed complex sequences of events with many properties which were similar to the one- and two-dimensional Burridge–Knopoff simulations.

Complexity has been particularly elusive for continuum simulations using the laboratory-based Dieterich–Ruina rate and state friction law [*Dieterich*, 1978, 1979; *Ruina*, 1983]. *Ben-Zion and Rice* [1993], *Rice* [1993], and *Rice and Ben-Zion* [1996] saw no evidence of slip complexity generated solely by nonlinear dynamics on smooth faults. They were, however, able to reproduce the broad distributions of events observed for the Earth by making their models inherently discrete or heterogeneous. Compared with the friction laws used in the continuum models studied by *Langer et al.* [1996] and *Cochard and Madariaga* [1994], similar models using the Dieterich–Ruina law do not exhibit as strong instabilities at high slipping speeds. More recently, *B.E. Shaw and J.R. Rice* (private communication, 1999) have observed complexity over a restricted range of parameters in a continuum model where the Dieterich-Ruina friction law is modified at high slip speeds to yield a greater instability.

While these results span a variety of behaviors, they do suggest that at least for a restricted range of parameters low-dimensional models and continuum models may yield qualitatively similar results. If that is the case, it could be useful. Our present computational limits combined with the broad range of scales present in seismology mandate use of a family of models, rather than a unique individual model, to address all of the most pressing issues. However, to date relatively little work has been done to evaluate the limitations of particular modeling methods or to develop systematic methods for incorporating the results of three-dimensional continuum models in simplified lower-dimensional (e.g., Burridge–Knopoff) models. In fact, few, if any, studies have been made in which the results of low-dimensional models and continuum models subject to the same friction law are directly compared.

We begin to address these issues by studying a three-dimensional scalar, continuum model and comparing its behavior to that observed in a one-dimensional Burridge–Knopoff (BK) model. For both the three-dimensional continuum model and the BK model, we focus on spatially homogeneous dynamical systems for which the friction is described by a rate and state law introduced in section 2. We investigate the sensitivity of large, propagating events to variations in the friction parameters. We also investigate the effect of varying the aspect ratio and expanding the fault size, while keeping the size of discrete cells constant and small. Our results suggest that in the continuum the large length scales (that is, the length and width of the fault) can play an important role in determining whether dynamical complexity is observed.

Our measurements include characterizations of single ruptures propagating through regions of homogeneous prestress, as well as classifying the patterns associated with recurrent ruptures. In one regime, we observe broad and periodic crack-like ruptures which heal in response to edge effects. In another regime we observe narrow, self-healing slip pulses which lead to dynamical complexity in sequences of repeated events.

The rest of this paper is organized as follows: In section 2 we introduce the rate and state friction law which we use in our simulations. In section 3 we describe

the continuum fault model and summarize the corresponding numerical results as the friction parameters and fault geometry are varied. In section 4 we describe analogous properties for the Burridge–Knopoff model. We conclude in section 5 with a summary of our results and discussion of open questions that remain.

2. Friction Law

Friction is a central ingredient in earthquake models. Relevant dissipation mechanisms include fracture, heat and deformation generated during sliding, and the dynamics of fluids and gouge. However, the manner in which these processes collapse into dynamic constitutive equations remains poorly understood. While dynamic inversions of a few well-monitored earthquakes are beginning to yield some constraints (e.g., on the characteristic displacements associated with frictional weakening [*Ide and Takeo*, 1997] and the absolute level of stress [*Spudich*, 1998; *Guatteri and Spudich*, 1998]), we are a long way from being able to measure friction at tectonic scales.

Limitations in our ability to resolve friction parameters from seismograms can be attributed to a variety of sources. These sources include resolution limits on available data sets associated with the inherent noise of seismic signals, computational and measurement limits on the representation of local geometries, and intrinsic uncertainties in initial conditions and geophysical parameters. None of these difficulties is likely to be eliminated in the near future. Thus we are left with a dilemma regarding how to proceed and, in particular, how to determine the best friction laws to use in models. The fundamental uncertainties make it necessary to study a variety of candidates and to determine in parallel which dynamical features depend sensitively on the details of the friction law and which do not.

For our studies we define a rate and state friction law which incorporates a characteristic distance δ for slip weakening, a characteristic time τ for healing, and a velocity-weakening steady state. We choose the simplest functional representation for these features. The friction $F(\Delta\dot{U},\theta)$ is given by

$$F = \begin{cases} [-\theta,\theta], & \Delta\dot{U} = 0; \\ \theta + \eta\Delta\dot{U}, & \Delta\dot{U} > 0, \end{cases} \tag{1}$$

where the state variable θ satisfies the evolution equation

$$\dot{\theta} = \frac{1-\theta}{\tau} - \frac{1}{\delta}\theta\Delta\dot{U}. \tag{2}$$

Here ΔU represents the relative local displacement of opposite sides of the fault (i.e., the slip), and the dot denotes a derivative with respect to time t. When the interface is stationary, $\Delta\dot{U} = 0$, the static friction threshold is set by the value of the state variable θ, which is confined to the unit interval $0 < \theta < 1$.

The steady state friction applies when there is a constant slip rate $\Delta\dot{U}_{SS}$. In this regime the state variable exhibits velocity weakening:

$$\theta_{ss} = \frac{1}{1+\Delta\dot{U}_{SS}\tau/\delta}. \tag{3}$$

When $\eta > 0$ the steady state friction $F_{SS} = \theta_{SS} + \eta\Delta\dot{U}_{SS}$ exhibits a crossover from velocity weaking to velocity strengthening at $\Delta\dot{U}_{SS} = (\delta/\tau)\,[(\tau/\delta\eta)^{1/2} - 1]$.

To illustrate the basic properties of this friction law, we first consider it in the context of a single slider block, attached to one end of a simple harmonic spring, which is pulled at the opposite end at uniform velocity V. The dimensionless equation of motion is

$$\Delta\ddot{U} = -(\Delta U - Vt) - F(\Delta\dot{U},\theta). \tag{4}$$

This mechanical system is a typical approximation for many laboratory friction experiments, in which slip occurs uniformly across the interface.

In Figure 1 we illustrate the evolution of the friction for the special case $\eta = 0$ (so that $F = \theta$) following step changes in the drive speed V for three different values of the slip-weakening length δ. For larger δ, F decays more slowly, and the steady state value is higher. Note the asymmetry between the frictional weakening and healing. When slip terminates, healing occurs at the same rate for all of the curves, since $\tau = 10$ in each case.

At sufficiently low drive velocities and stiffnesses, equation (4) exhibits stick-slip solutions. In Figure 2 a we plot the slider velocity $\Delta\dot{U}(t)$ and state variable $\theta(t)$ for the same friction parameters used in Figure 1. At the onset of motion, θ drops sharply over a characteristic distance which scales with δ, from an initial value close to the maximum value of unity (which will always be true at the onset of slip in the slow drive rate limit). As θ drops, $\Delta\dot{U}$ increases, such that the minimum value

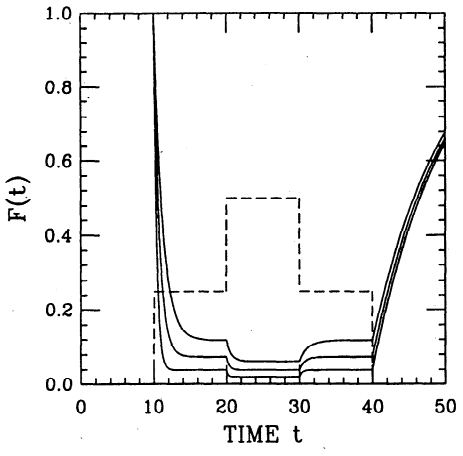

Figure 1. Transient response of friction to step changes in the drive velocity (dashed line). We observe frictional weakening over a characteristic displacement δ and strengthening over a characteristic time τ. For each of the curves, $\eta = 0$ and $\tau = 10$. From top to bottom the solid curves correspond to slip-weakening length $\delta = 0.33$, 0.2, and 0.1. As δ decreases, the transient period associated with frictional weakening becomes shorter and the steady state friction decreases.

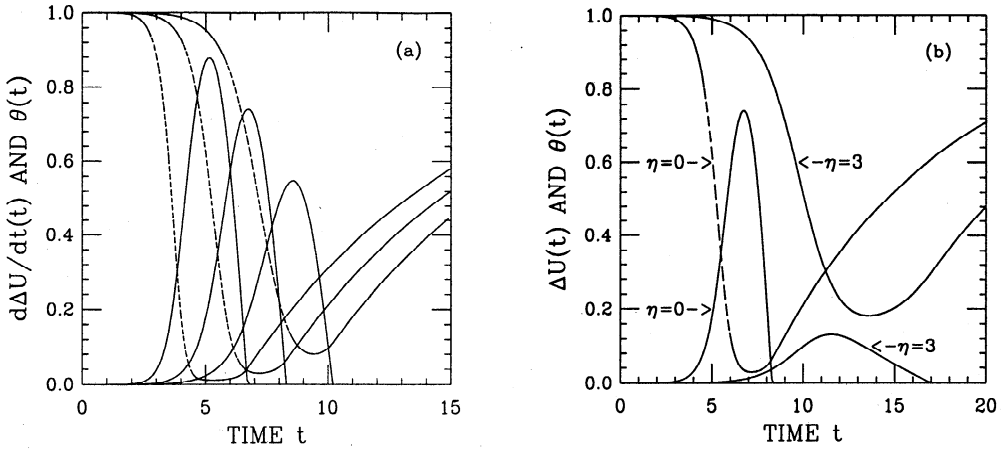

Figure 2. Periodic stick-slip solutions. We set the stiffness $k = 1$ and the velocity $V = 0.001$. (a) Results for the slip rates (solid lines) and state variables (dotted lines) for the same friction parameters used in Figure 1. Each slip pulse begins at time $t = 0$. Larger values of δ are associated with suppressed amplitude and increasing time delay in the peak velocity. (b) contrast of the underdamped ($\eta = 0$) and overdamped ($\eta = 3$) results for $\delta = 0.2$ and $\tau = 10$. In the underdamped case the duration of appreciable slip velocity is of order the inertial time (π in our dimensionless units), while in the overdamped case the slipping time is significantly longer and depends on the friction parameters.

of θ occurs near the maximum $\Delta\dot{U}$. After reaching the peak value, $\Delta\dot{U}$ decays at a rate which depends on the damping η and the healing rate τ. In each case, increases in the slip-weakening length δ or decreases in the healing time τ result in a suppression of the slip amplitude. Because the slider is underdamped ($\eta = 0$ in Figure 2 a), the slip time is roughly equal to the inertial time, independent of the friction parameters. Slip terminates abruptly, at which point the healing rate increases. In contrast, as illustrated in Figure 2 b, when the system is overdamped ($\eta > 2$), the slip rate decays more gradually until the block resticks. For overdamped solutions, the slip time does depend on the friction parameters. In each case, the displacement and maximum velocity associated with an individual slip event increases with decreasing δ and increasing τ, which both result in an overall reduction of the dissipation.

In Figure 3 we plot the friction force $F = \theta + \eta\Delta\dot{U}$ versus the instantaneous velocity $\Delta\dot{U}$ for the slip events illustrated in Figure 2 b. The solutions differ significantly from the steady state (single-valued) friction laws which are also shown. The steady state curves exhibit velocity weakening at low speeds, crossing over to velocity strengthening at high speeds when $\eta > 0$. In comparison, in the slip-weakening phase the solution to (4) exhibits a much more gradual decay in the force as the speed increases in comparison with the steady state. When the block resticks, the state variable has not fully healed, so that initially the static friction is significantly lower than the maximum value of unity.

The parameter values used in Figure 2 are representative of one generic class of behavior for the model. We have chosen δ to be small enough that slip weakening occurs over a length that is small in comparison with the full slip distance, and we have chosen τ to be large enough that healing does not interfere significantly with the slip weakening phase. Comparing underdamped ($\eta = 0$) and overdamped ($\eta = 3$) solutions has a special significance for the sections that follow. Introducing the viscous damping term $\eta\dot{U}$ into the one-dimensional BK model which is often defined without it will serve as an approximate method of represent-

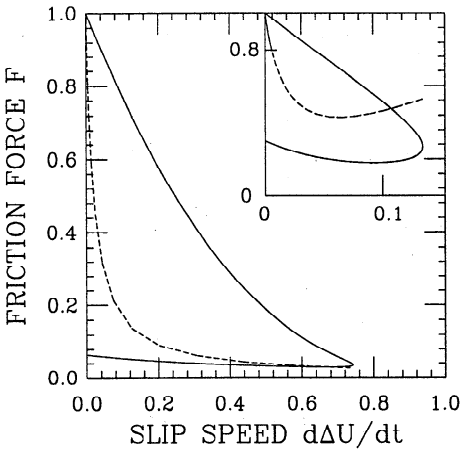

Figure 3. Friction hysteresis: during the stick-slip cycle the rate and state friction (solid curves) does not resemble the steady state evaluated at the instantaneous slip rate (dashed curves). The two sets of curves represent the stick-slip solutions shown in Figure 2b, with the main curve corresponding to the underdamped solution ($\eta = 0$) and the inset corresponding to the overdamped case ($\eta = 3$). The shape of the hysteresis loop depends on the friction parameters. A decrease in δ extends the loop, while a decrease in τ leads to more significant healing as $\Delta\dot{U} \to 0^+$.

ing the dissipation associated with loss of energy to the surrounding medium that arises even with $\eta = 0$ in the three-dimensional continuum model [*Knopoff et al.*, 1992].

Our friction law differs significantly from the commonly studied Dieterich–Ruina rate and state law [*Dieterich*, 1978, 1979; *Ruina*, 1983] which has been studied extensively in the context of laboratory experiments [*Rice and Ruina*, 1983; *Rice and Tse*, 1986; *Dieterich and Kilgore*, 1994; *Tullis and Weeks*, 1986; *Marone and Kilgore*, 1993] and applied to earthquake models by *Rice* [1993], *Rice et al.* [1994], and *Dieterich* [1994]. The Dieterich–Ruina law involves a much more gradual logarithmic dependence on the slip rate and state variable. The logarithmic dependence of the friction is consistent with laboratory measurements for quasi-static deformation of dry interfaces with micron-scale roughness.

We define our friction law primarily on the basis of its simplicity, though there are similarities between it and other constitutive relations which have recently been considered. The initial slip-weakening phase and the form of the velocity-weakening steady state resemble those of the piecewise continuous friction law considered by *Cochard and Madariaga* [1994], which is defined explicitly in terms of slip and slip rate rather than a state variable. Our law also resembles a rate and state law derived for boundary lubrication [*Carlson and Batista*, 1996], with a mechanism involving a shear melting transition of the lubricant [*Thompson and Robbins*, 1990], and has some features in common with forms previously described by *Sibson* [1982], *Lachenbruch* [1980], and *Shaw* [1995], where the mechanism for frictional weakening is the reduction of normal force as a consequence of heating and expansion of fluids. It is interesting to note that in both boundary lubrication and the models of friction at faults which incorporate fluids, the dissipation mechanism is associated with state transformations of intermediate materials, which result in dilatancy and ultimately reductions of friction due to disorder. However, it remains an open problem to connect laboratory friction measurements to processes which occur on seismic scales. In typical laboratory experiments the pressures, slip rates, and system sizes are orders of magnitude less than those of faults.

3. Continuum Model

Earthquake faults are complex and comparatively weak interfaces embedded in the Earth's crust. The dynamic rupture and frictional sliding which occur on the fault are coupled to the surrounding medium via redistribution of stress and radiation of seismic energy. In addition to describing the friction and dynamics of the fault, a realistic earthquake model should account for this coupling.

In this section we define the three-dimensional continuum model (section 3.1) used in the bulk of our studies and explore its behavior in the context of two classes of numerical experiments. They include (1) individual ruptures which initiate at an asperity and propagate through regions of homogeneous prestress (section 3.2) and (2) recurrent ruptures in systems with inhomogeneous initial conditions (section 3.3). For both cases we consider the effects of varying the friction parameters, the overall system size, and the aspect ratio of the fault.

3.1. Numerical Methods

Because we emphasize dynamical effects, we take the simplest geometric representation: a fault consisting of a planar interface embedded in homogeneous material. Absorbing boundary conditions surround the system to prevent waves which radiate from the fault from reflecting back toward the interior.

While some authors have investigated recurrent ruptures on faults embedded in fully elastic media [*Nielsen et al.*, 1995; *Cochard and Madariaga*, 1996; *Ben-Zion and Rice*, 1997], we take the approach suggested by *Burridge and Moon* [1981] in which the elastic medium is replaced by an analog scalar medium. In this analogy, we solve for a scalar displacement U and a vector stress σ_i, which satisfy

$$\frac{\partial}{\partial t}\dot{U} = \frac{1}{\rho}\frac{\partial}{\partial x_i}\sigma_i\,; \qquad \sigma_i = \mu\frac{\partial}{\partial x_i}U, \tag{5}$$

where μ is the stiffness and ρ is the density of the medium. On the fault plane, we take σ_1 to be the stress component which is equal to the friction (equation (1)). Since only σ_1 appears in the remaining discussion, from now on we will omit the component subscript.

While the simplification to scalar displacements leaves out features of the complete three-dimensional elastodynamics which are important for direct comparisons with seismograms, it has the advantage of eliminating much of the tensor complexity of the problem. The number of field variables which are solved for at each node is dramatically reduced, allowing us to implement larger and longer simulations. In addition, the anisotropy which is due to the variable angle between the direction of rupture propagation and slip is eliminated in this formulation because slip is a scalar. This allows us to focus more directly on the influence of friction on rupture without the additional complexity associated with anisotropy. We have performed several simulations for the tensor elastodynamic case to verify that our basic conclusions extend to this regime. A more complete study of tensor elastodynamics will be the subject of a later publication. We emphasize that in certain cases, scalar models can give the same results as tensor ones. For example, a circular crack expanding at constant velocity yields the same slip function for both the fully elastic medium and the scalar approximation, in the form $A[t^2 - (r/c)^2]^{1/2}$, where r is the distance from the nucleation. The amplitude factor A depends on medium parameters and rupture velocity c [*Burridge and Moon*, 1981]. In the elastic case the

function above defines slip in the direction of the fault initial shear traction; slip in the perpendicular direction may occur in the elastic medium but can be shown to be negligible for homogeneous prestress [*Madariaga*, 1976]. Surprisingly enough, the slip function is isotropic even in the fully elastic case provided that the front is circular. Therefore in certain cases a scalar model can be a surrogate for the more intricate elastic model, particularly in problems where anisotropy of the rupture and rake rotation play negligible parts.

The algorithm we use to solve equation (5) is inspired in part by the adaptation of fourth-order finite differences proposed by *Madariaga et al.* [1996]. However, we use an alternative approach to describe the embedded interface which makes use of analytical solutions in order to improve the accuracy. From Betti's Representation Theorem [*Aki and Richards*, 1980], the stress on the fault can be expressed in terms of the instantaneous local slip velocity $\Delta\dot{U}$ and a long range elastic stress σ_e:

$$\sigma(\mathbf{x},t) = -\frac{\mu}{2\beta}\Delta\dot{U}(\mathbf{x},t) + \sigma_e(\mathbf{x},t) + \sigma_0(\mathbf{x}). \quad (6)$$

In this equation, σ_0 is the intial stress distribution at the onset of fracture. Here σ_e is the cumulative nonlocal contribution to the stress, mediated by the surrounding elastic medium, which results from slip that occurs on any segment of the fault up to time t. Finally, $\sigma(\mathbf{x},t)$ is the friction $F(\mathbf{x},t) = F(\theta(\mathbf{x},t), \Delta\dot{U}(\mathbf{x},t))$ (equation (1)). In the boundary integral method, σ_e is computed explicitly as an integral over space and time [*Cochard and Madariaga,* 1994]. As shown by *Nielsen and Olsen* [1998], it is possible to use the theorem in the finite difference scheme by updating the stress and the displacement rates based on the stress and displacement gradients from the previous time step as described by equation (5) and then correcting the slip rates for the additional dissipation due to friction using equation (6). The procedure is straightforward, since σ_e is implicitly calculated when the stress is computed by finite differences without the need to explicitly compute a complex convolution in space and time.

The development of reliable numerical methods has been a key factor enabling us to draw conclusions regarding dynamical complexity in the continuum model and the sensitivity of our results to variations in the friction law. We observe an improvement over our previous modeling in which Betti's Representation Theorem is not explicitly incorporated into the numerical algorithm but rather results implicitly from the dynamical equations. In particular, the numerical noise, in the form of spurious oscillations, is considerably reduced. The manner in which the discontinuity of displacement is defined allows us to clearly distinguish between the elastic and dislocation contributions to the deformation and does not preclude the use of higher-order spatial derivatives in the numerical grid [*Nielsen and Olsen*, 1998].

In the remainder of section 3, we obtain numerical solutions for the continuum model with zero viscosity ($\eta = 0$ in equation (1)) and in dimensionless units, setting $\mu = \rho = \beta = \sigma_{\max} = 1$. We have run simulations for small finite values of η (of the order of 0.01) and obtained essentially identical results. To relate our results to observations, we can reintroduce the dimensional variables, where the slip, slip rate, wave speed, and stresses are related to characteristic values for the Earth. They are calculated on the basis of typical shear wave speeds (β) of the order of 3000 m/s, typical densities (ρ) of the order of 3000 kg/m^3, and typical slip rates ($\Delta\dot{U}$) of the order of 1 m/s. The fact that $\beta = (\mu/\rho)^{1/2}$ yields an estimate of the stiffness $\mu = 2.7 \times 10^{10}$ Pa. Furthermore, the characteristic velocity of the medium (see section 3.3) is related to the stress drop by $\Delta\dot{U} = \Delta\sigma\beta/\mu$, so that $\Delta\sigma$ is of the order of 9×10^6 Pa.

3.2. Single Rupture With Homogeneous Prestress

Our first step in analyzing the continuum model is to study simple symmetric solutions for slip propagating through regions of homogeneous prestress. We bypass the details of nucleation and focus instead on properties of well-developed ruptures. In each simulation, we begin with an initial configuration in which the stress on the fault is homogeneously set at 45% of the fracture yield stress, except for a small circular asperity of radius 10 nondimensional units. Inside the asperity the prestress is set just above the rupture threshold, so that this region breaks immediately at time $t = 0$, providing a finite nucleation patch for the event.

In Figure 4 we illustrate the time-dependent velocity and friction at a fixed location as the rupture passes through. Our results correspond to three different values of δ ($\delta = 0.1, 0.2$, and 0.33), with the healing time τ held constant ($\tau = 10$). The fact that onset of slip is increasingly delayed with increasing δ reflects the fact that the fronts propagate slower for larger values of the slip-weakening length.

The basic shape of the slip rate curves in Figure 4 can be broken up into three stages. Initially, the slip rate increases abruptly but continuously while simultaneously the friction drops rapidly over the characteristic length δ. At intermediate times the velocity relaxes from the sharp maximum to an almost constant value. Finally, there is a turnover in the slip rate, and sliding ends abruptly. In the final stages of slip, rate-weakening allows friction to rise to higher values; however, recovery of the full frictional strength takes place mostly after stick is initiated, over the characteristic time τ.

It is instructive to compare our ruptures to the classical Kostrov solution for an expanding crack of fixed propagation velocity in a medium characterized by a constant breaking strength but no dynamic friction [*Kostrov*, 1964]. At the onset of motion, Kostrov cracks

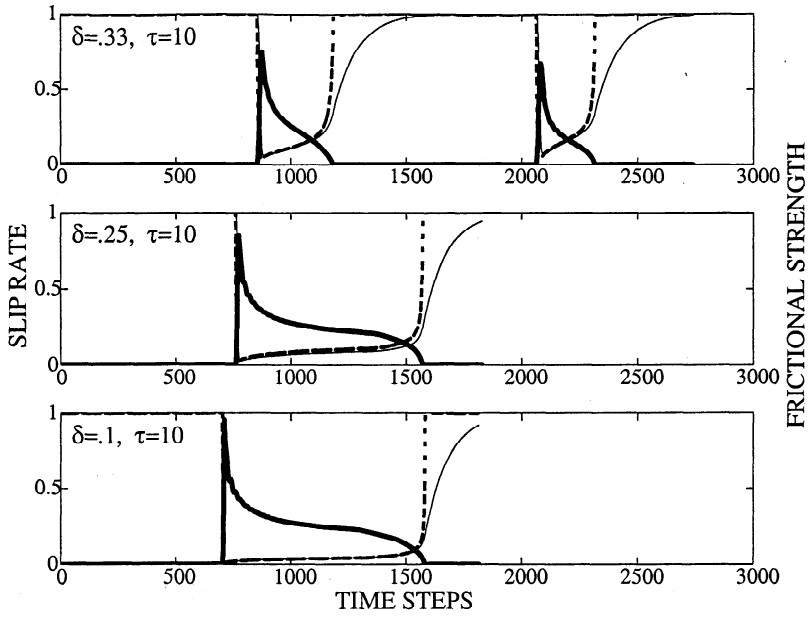

Figure 4. Local values of the slip rate (thick curve), friction (thin curve) and corresponding steadystate friction (dashed curve) for a sample point in the continuum model during rupture propagation through a region of homogeneous prestress. The initial conditions are fixed for the three cases, and τ is held constant, while δ is varied as indicated. In each case the dynamic stress drop is of order $\Delta\sigma \approx 0.45$. The recovery of frictional strength (thin curve) is similar in the three cases; however, healing occurs earlier for larger δ, leading to a shorter rise time. The repeated slip for $\delta = 0.33$ indicates a second rupture of the fault in the absence of reloading. The true friction is nearly equal to the steady state except at the onset and termination of active slip. Total fault size is $(140, 140)$ lattice units, spatial sampling is 1, and time sampling is 0.1. The sample point is located at $(35, 35)$, and the nucleation is centered at $(90, 90)$.

exhibit an unphysical stress singularity at the crack tip, which results in a $1/\sqrt{t}$ divergence in the slip rate. By incorporating a characteristic slip-weakening length δ we remove the singularity, which leads to more physical solutions.

The intermediate portions of the slip rate curves in Figure 4 more closely resemble Kostrov solutions, except for very high values of δ/τ where the pulse is too narrow for an intermediate phase to develop. The decay from the peak slip rate toward a nearly constant value roughly mimics the $1/\sqrt{t}$ dependence. However, unlike Kostrov cracks which expand indefinitely (in an infinite medium) and never heal, our ruptures end abruptly and the interface resticks.

For $\delta = 0.1$ and 0.2 healing occurs only after the front edge of the rupture has reached the unbreakable boundaries, which results in a resticking front which propagates back toward the center of the fault. In this case, the rise time (average local slip time) is controlled by the size of the fault. In contrast, when $\delta = 0.33$, we begin to observe spontaneous healing, independent of the boundary. In the particular case illustrated in Figure 4 a second rupture is triggered from the initial nucleation site. Because the system is not actively loaded during sliding, the stresses which trigger the second rupture are associated with long-range radiation and stress redistributions which result from slip on other portions of the fault. This cannot occur in crack-like regimes or in models that lack long-range elastic radiation. Retriggering is facilitated in this case because the residual stress after rupture is relatively high, a feature due to the presence of rate weakening and the high δ/τ ratio that was used. In other words, a shorter rupture pulse generates a reduced slip and a reduced stress drop, so that the fault remains close to the yield threshold after rupture.

In Figure 4 we compare the steady state friction θ_{SS} (equation (3)) with the instantaneous friction θ. For each value of δ through most of the rupture the two curves are essentially indistinguishable. However, during the initial and final stages of slip where the velocity is changing rapidly, the detailed evolution of the state variable becomes important and the two curves differ markedly. This is illustrated in Figure 5, where we show that θ and θ_{SS} are dramatically different when viewed as a function of slip rate, as we observed previously for the single slider solutions in Figure 3.

In order to evaluate more systematically the consequences of varying the friction parameters, we have run simulations of the 25 combinations of $\delta = [1.8, 1.85, 1.9, 1.95]$ and $\tau = [45, 46.25, 47.5, 48.75, 50]$, with a fixed prestress $\sigma_0 = 0.45$. Snapshots of the results for the different (δ, τ) pairs are illustrated in Figure 6. For each pair the velocity of the actively slipping

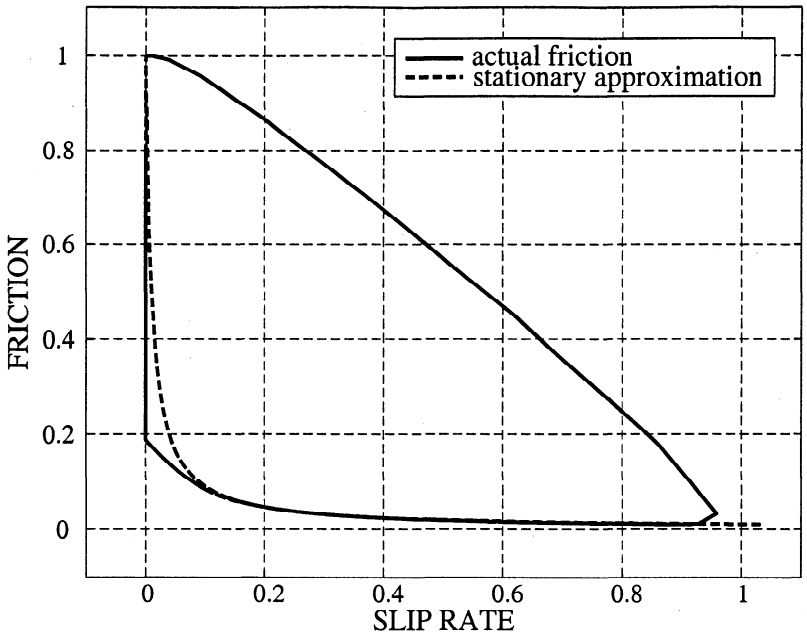

Figure 5. Friction hysteresis in the continuum model. The solid curve corresponds to the friction θ plotted as a function of the instantaneous displacement rate $\Delta\dot{U}$ at a specific location on the fault. The data shown correspond to the same simulation illustrated in the bottom curve in Figure 4. The result is compared with the corresponding value of the steady state friction (dashed curve) for the same value of $\Delta\dot{U}$. The two curves overlap except for the initial phase (where the true friction is stronger owing to the slip weakening onset) and the final phase (where the true friction is suppressed relative to the steady state due to the delay associated with time-dependent healing).

patch on the fault after 140 dimensionless units of time is shown. Darker regions in gray scale represent faster slip rates. The distance between the outermost slipping site and the central asperity is referred to as the rupture radius. Larger values of the rupture radius at fixed time (as in Figure 6) correspond to faster propagation rates. The radial difference between the outermost and innermost actively slipping sites measured with respect to the center of the circular asperity is the instantaneous rupture width. In Figure 6 we see a great deal of variation in this quantity. In the upper left-hand corner the slipping region is a solid, circular disk, corresponding to crack-like ruptures. Moving toward the lower right-hand corner, the ruptures become increasingly narrow and pulse-like, until finally the rupture fails to propagate.

These variations are evaluated quantitatively in Figure 7, where we plot the rupture width averaged over the fault area and the duration of each event. The rupture width is roughly constant along the diagonal lines. Variations in average rupture width are also system size dependent. This is a priori true for crack-like solutions, in which healing does not begin until the outermost edge of the rupture encounters the boundary. Even the narrow, self-healing pulses do not represent stationary solutions for the system sizes we can consider. In this case, the rupture width also increases as slip propagates toward the boundary. These expanding pulse solutions will be investigated in detail in a future publication. The averages plotted in Figure 7 combine the properties of the solutions as they evolve from the initial asperity triggered nucleation until slip has fully terminated, and the specific values obtained for the rupture width increase with increasing system size.

For the range of parameters that we have chosen the fact that the contours of constant rupture width in Figure 7 are roughly diagonal in the δ versus τ plane is consistent with a rupture width that varies more systematically with the ratio δ/τ than with independent variation of either parameter. This ratio has the dimensions of a velocity and appears in equation (3) as the characteristic velocity of the steady state friction. As is illustrated in Figure 4, the actual friction coincides with the steady state value during most of the active phase, except for the initial and final portions in which the velocity changes rapidly (Figure 5). Once the slip rate drops below a characteristic value that scales nonlinearly with δ/τ, we observe the rapid onset of stick. Within the parameter range discussed here, this characteristic healing rate is of the order of 10 times δ/τ; its precise expression is a function of δ, τ, β, μ, whose derivation is beyond the scope of this paper but will be discussed elsewhere. If this occurs before the rupture front reaches the boundary, we obtain narrow, self-healing slip pulses. Alternately, crack-like solutions occur when ruptures reach the boundary first.

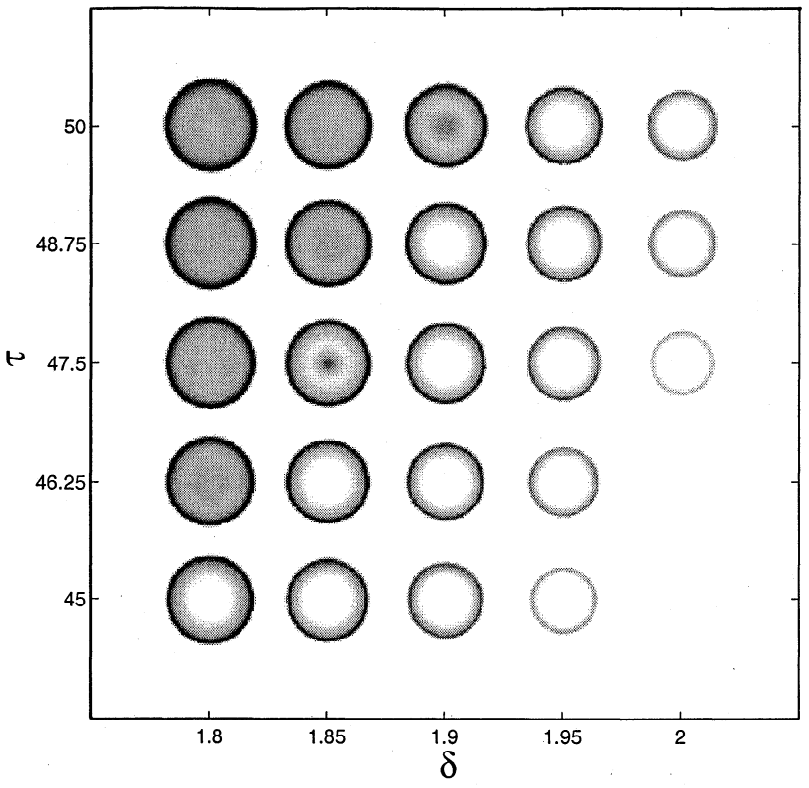

Figure 6. Spatial variations of the slip velocity at fixed time after nucleation for different values of (δ, τ). The circular patterns represent the actively slipping area after 140 dimensionless units of time. Each snapshot is centered on the (δ, τ) value which was used to produce it. Variations in both the overall radius (indicative of different rupture propagation velocities) and the width of the actively slipping region (i.e. rupture width) are observed. Note that the similarity in the patterns persists along the diagonal lines. The dynamic stress drop is $\Delta\sigma \approx 0.45$ in all the simulations.

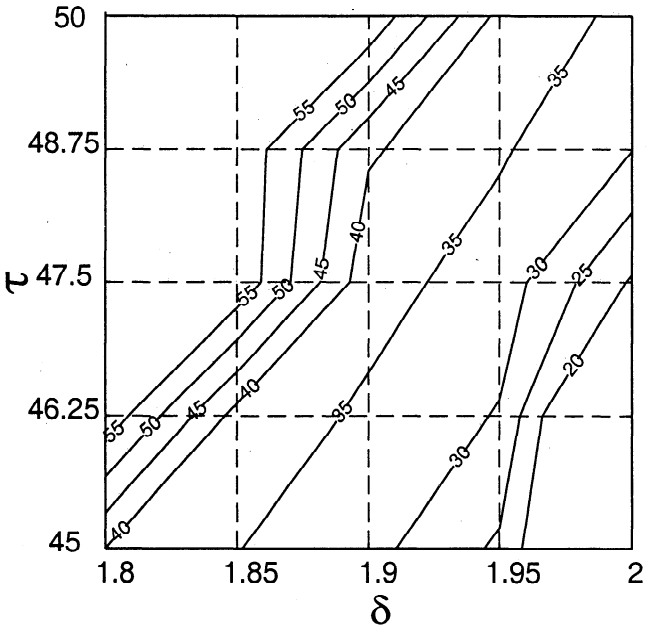

Figure 7. Contours of constant rupture width, in lattice units, plotted as a function of δ and τ. These values represent time-averaged values over the duration of rupture for the same set of simulations illustrated in Figure 6.

This result is consistent with results based on piecewise continuous slip- and rate-weakening friction by *Cochard and Madariaga* [1996], where larger values of the frictional characteristic velocity also led to the formation of self-healing pulses. As in the single-slider solutions (Figure 2), larger values of δ suppress slip at the onset of sliding, while smaller values of τ lead to more rapid healing. Because we have focused on parameter regimes in which τ is long in comparison with the time over which slip comes to arrest, relatively little strengthening takes place during slip. Instead, most of the strength is restored during the recovery phase, which takes place after slip terminates. Because we study the seismically relevant case in which the loading rate is taken to be infinitesimal, healing during the stick phase is complete, except in cases involving secondary ruptures as illustrated in the top of Figure 4. On the other hand, in systems that are loaded at much faster rates (as in laboratory experiments), the strength recovery rate plays an important role.

Finally, we comment on the effects of varying the system size and aspect ratio. When the system size is varied for a square fault, it is possible to reduce the size of the fault and obtain a crossover from narrow pulses to the crack-like regime when the fault size becomes com-

parable to the rupture width. As was described above, if the crack reaches the barriers while the interior is still in motion, healing is triggered primarily by the boundaries of the fault.

If the fault width is more than the spontaneous width defined by δ/τ, the rupture width is essentially independent of the fault dimensions (see Figure 8). In contrast, when the fault width is less than the spontaneous width defined by δ/τ, the shortest linear dimension (which we take to be the fault width) controls the rupture width. Interestingly, in the continuum models we observed the propagation of stationary slip pulses only for high aspect ratios. For square faults in the crack-like regime, the slipping region expands until the front reaches the boundary, at which point a healing wave begins to propagate back toward the interior. Even the narrow, self-healing pulse solutions become progressively wider as they propagate toward the boundary. Only when the rupture width is determined by the shortest linear dimension does it approach a stationary value.

While these results suggest that the distinction between crack-like and self-healing ruptures is determined at least in part by δ/τ, this ratio only becomes physically meaningful when it is scaled by an appropriate velocity of the medium. We define a dimensionless ratio $(\mu\ \delta)/(\Delta\ \sigma\ \beta\ \tau)$ by scaling δ/τ with the characteristic velocity of rupture in a homogeneous medium of stiffness μ, wave velocity β, and a stress drop $\Delta\sigma$. We define $\Delta\sigma$ as the dynamic stress drop (i.e., the difference between the prestress σ_0 and the friction during active sliding). Dimensional arguments lead to the estimate $\Delta\dot{U} \approx \Delta\sigma\beta/\mu$, supported by analytical solutions (see, for example, *Dahlen* [1974], for an elliptical crack with prescribed propagation velocity). While $\Delta\sigma$ is a variable that depends to some extent on δ/τ, we verify that the sliding friction is relatively low during most of the active phase. Consequently, we can assume that $\Delta\sigma$ is approximately equal to the prestress σ_0 in our computations. This approximation yields an estimate of the characteristic slip rate which is independent of the rate and state friction parameters.

Small values of δ/τ correspond to the crack-like regime in section 3.2. Alternately, large values of δ/τ correspond to the regime where self-healing pulses are observed. We have performed some preliminary studies in which we vary the prestress, and thus $\Delta\sigma$, for fixed friction parameters. These results are consistent with a crossover between crack-like and self-healing ruptures which varies inversely with prestress. Our results also agree qualitatively with a more detailed analysis of the crossover from crack-like ruptures to self-healing rupture performed by *Cochard and Rice* [1997] for the case in which the friction is described by a simple velocity weakening law analogous to our equation (3). For our friction law, our estimate of the crossover does not lie within the quantitative bounds set by Cochard and Rice for velocity-weakening friction. The discrepancy is of the order of a factor of 2.

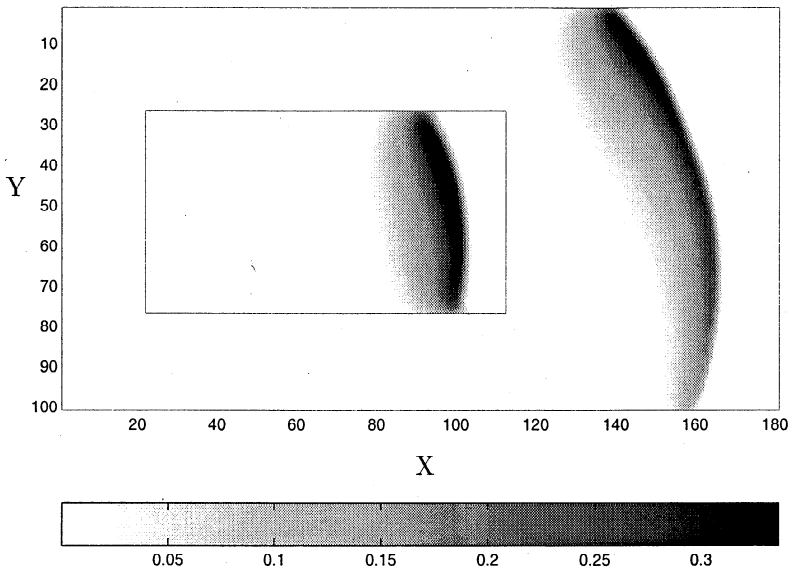

Figure 8. Examples of rupture widths that are independent of the fault size. Darker shades correspond to higher slip rates within actively propagating ruptures on faults of two different sizes. The outer perimeter marks the edge of the unbreakable barriers. These snapshots are extracted from a series of recurrent ruptures and are representative of typical events. The width of the darkened region is roughly the same for the two cases.

3.3. Recurrent Ruptures

Next we focus on recurrent ruptures. We initialize the system in the same asperity state considered in section 3.2 (after an initial transient period, the results are qualitatively insensitive to the details of the initialization). We simulate a sequence of large events by reloading the fault once each rupture is terminated and the radiated waves have propagated to the absorbing boundaries. The final state of stress on the fault is used as the initial condition for the next rupture, after increasing the load sufficiently to induce nucleation of the next event.

If we load the fault at a continuous and infinitesimal rate, we can capture the full evolution of each event. However, in the regime where we observe dynamical complexity, small events consume the bulk of our computational resources, preventing us from considering enough consecutive large events to conclude that we are beyond the initial transient. Thus in order to maximize the number of large events we can consider, we again focus on the later stages of well-formed ruptures and ignore both the details of initiation, as well as events of small and moderate size. To do this, we define a nucleation criterion based on a comparison between the maximum value of the available elastic energy E_e in a connected patch on the fault and the fracture energy E_f associated with generating slip of the order of δ within the patch. Here we define E_e to be

$$E_e = \sum_{n=1}^{N} \frac{1}{\mu} \sigma^2(n) dx^3, \tag{7}$$

where σ is the shear stress, n is the index of the discrete fault element inside an overstressed patch of N elements, μ is the stiffness, and dx is the side of one element. We estimate E_f in terms of the work required to overcome a piecewise linear slip-weakening friction law, characterized by the slip-weakening distance δ:

$$E_f = \sum_{n=1}^{N} \frac{1}{2} \left(\sigma_y(n) - \sigma_d(n)\right) \, \delta \, dx^2 \, , \tag{8}$$

where σ_y is the yield stress and σ_d is an estimate of the dynamic frictional stress. Alternatively, we could consider a propagation criterion, in which we compare the elastic energy dE_e/dR released when the radius R of the slip zone is increased with the fracture energy dE_f/dR required for slip to propagate into the expanded region. In our simulations the nucleation and propagation criteria are equivalent up to a constant.

When the elastic energy is large in comparison with the fracture energy, slip triggered by the asperity will typically develop into large propagating ruptures. Alternatively, when the elastic energy is small in comparison with the fracture energy, the event tends to die out rapidly without propagating. Our nucleation criterion is defined in terms of an adjustable parameter C, such that the load is increased uniformly until there exists a connected, overstressed patch in which

$$E_e \geq C E_f. \tag{9}$$

Adjusting C varies the size of the smallest event. In this manner we can test whether our results are sensitive to the details of nucleation. We may think of C as a geometrical correction (of order unity) which reflects the fact that asperities of different shapes will require different energies to propagate. Introducing an explicit shape dependence to the geometrical correction is complicated by the fact that the patch geometry is variable, nontrivial, and a priori unknown. After a few trial runs, we settled for a constant correction of $C = 0.4$ for which the number of aborting nucleations was seen to be reasonably reduced, while the generation of multiple simultaneous nucleation patches is extremely rare.

In studying recurrent ruptures, our primary goal is to distinguish between regimes (friction parameters and geometries) which lead to periodic behavior in which large events repeat at regular intervals and span the system and those which lead to complexity in the sequence of large events. Our operational definition of dynamical complexity corresponds to a self-sustained sequence of large events of a wide range of sizes and irregular recurrence intervals, which arises as a consequence of dynamically generated heterogeneity in the stress field. We emphasize that because we use a nucleation criterion aimed at creating asperities which generate large events, we restrict our attention to large-event complexity, as opposed to focusing on the population of smaller events.

In our simulations we typically first observe a transient phase, consisting of a series of quasi-periodic ruptures extending throughout the fault. We focus on the statistically stationary behavior (after roughly 10 large ruptures) to determine how the friction parameters and system geometry affect the level of complexity. We distinguish between three different regimes that can develop in a system of fixed size which are associated with increasing levels of heterogeneity in the stress field. These are strict periodicity, aperiodic systemwide events, and dynamical complexity. We have not obtained sharp estimates on crossover values of δ/τ which separate the different regimes. The appropriate values will depend on system size and prestress and would require extensive numerical computation to accurately characterize.

1. Regarding periodicity, for $\delta/\tau \approx 4 \times 10^{-3}$ and below we observe periodic large events, which generate smooth, repeating stress fields. Beginning from a random initial state, the system settles into a periodic state after a few cycles of large events. The particular features of the individual periodic large event depend on the initial state, though the general property of periodicity does not. While it is impossible to conclude from our simulations that the state does not evolve at all with time, we have observed events which repeat over 40 cycles, in which the difference between consecutive events (measured by the difference in slip summed over

the fault) decays exponentially with the cycle index. The periodic state is associated with broad crack-like ruptures, where healing occurs in response to boundary effects. Interestingly, in previous studies by *Nielsen et al.* [1995] in two dimensions for dynamic rupture under a time-dependent frictional weakening and by *Rice* [1993] in two dimensions for quasi-static rupture under a Dieterich–Ruina rate and state friction law, periodic states were associated with a stabilizing and smoothing effect which arose when frictional weakening occurred over large displacements. In our case, periodicity emerges for small slip-weakening lengths δ or, alternatively, large healing times τ. This occurs because it is easier for the rupture to propagate into new regions for smaller values of δ, while large values of τ (small δ/τ ratio) tend to suppress self-healing.

2. With respect to aperiodic systemwide events, for intermediate values of δ/τ, e.g., $\delta/\tau \approx 8 \times 10^{-3}$, we observe aperiodic large events which span the system, generating smooth but variable stress fields. The nucleation sites and dynamical evolution of the individual large events vary. As in the case of periodicity, the large events consist of crack-like ruptures. Moreover, clusters of small events start to appear that are due to aborted nucleations that did not trigger any rupture propagation.

3. Regarding dynamical complexity, for large values of δ/τ, e.g., $\delta/\tau \approx 6 \times 10^{-2}$ and above, we observe a broad distribution of sizes of large events and a highly heterogeneous and variable stress field. In this regime we observe narrow, self-healing slip pulses. For larger values of the slip-weakening length δ it is difficult for the rupture to propagate into fresh territories, while for smaller values of τ (larger values of the healing time δ/τ) healing takes place more rapidly. In this regime the stress field develops strong heterogeneities where the narrow pulses arrest, as illustrated in Figure 9. This sharp feature separates the patch which actively slipped from the patch which did not slip (where the stress is somewhat increased owing to long-range elastic effects). The narrow peaks of high stress typically comprise the nucleation sites of subsequent ruptures, and the stress heterogeneities sustain the broad distribution of events.

Because of such sharp features in the stress field, we begin to encounter problems with numerical accuracy in the regime where we observe dynamical complexity. To test the reliability of our results in this regime, we performed a series of simulations with increasing temporal and spatial accuracy. Final stress fields (a much more sensitive measure than displacements) for simulations with the same initial state but with two different grid spacings are illustrated in Figure 9. In both cases, the results include a sharp quasi-singular stress peak which is formed at the edge of the region which slips in the event and which can only be relatively sparsely sampled by the numerical grid. While the rupture front can be regularized using a gradual (slip-weakening) friction drop, there is no comparable control for the recovery of stiction. Indeed, stiction resumes most abruptly in the case of rate-weakening friction. As commented by *Cochard and Madariaga* [1994], the onset of stick occurs with an instantaneous jump from finite slip rate value to zero slip rate in the presence of rate-weakening (equation (3)). When the friction undergoes a less trivial evolution following the form of equation (1), the strength recovery can be made arbitrarily slow by increasing the

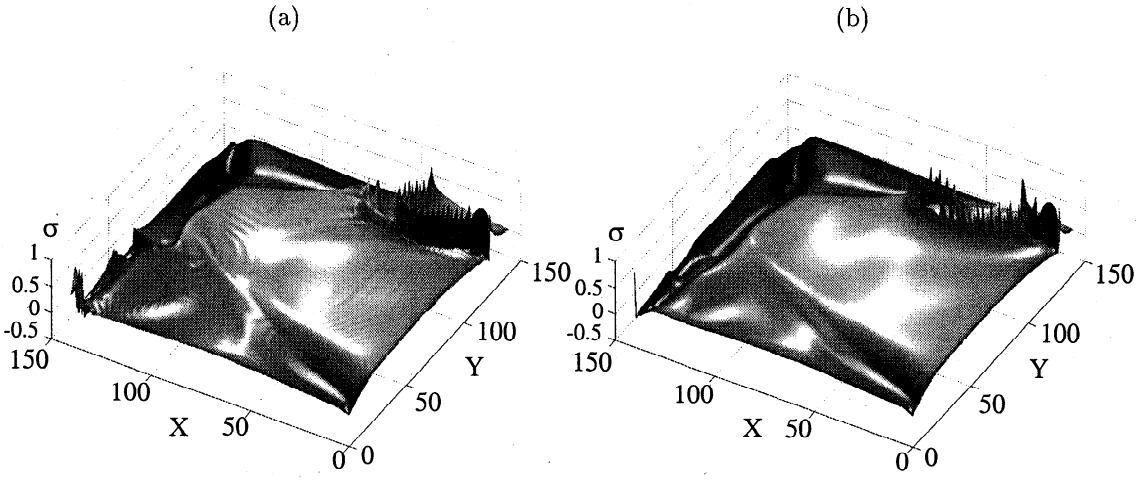

Figure 9. Stress field following a large event in the dynamically complex regime. Results obtained for the same initial conditions with two different grid sizes are shown. (a) A coarser grid ($dx = 1$) and (b) a finer grid $dx = 0.5$. The long-wavelength features are similar in the two cases. Some oscillations have disappeared in the finer gridding, and the peak in the stress field has shifted somewhat. The parameters for these simulations are $\delta = 0.66$, $\tau = 10$, with a dynamic stress drop $\Delta\sigma \approx 0.45$. A connected surface of $\approx 85\%$ of the total fault surface failed in both cases. The remaining 15%, located around the corner $(x = 0, y = 150)$ and surrounded by the stress peak, remained essentially unfractured for Figure 9b, but failed in part for Figure 9a.

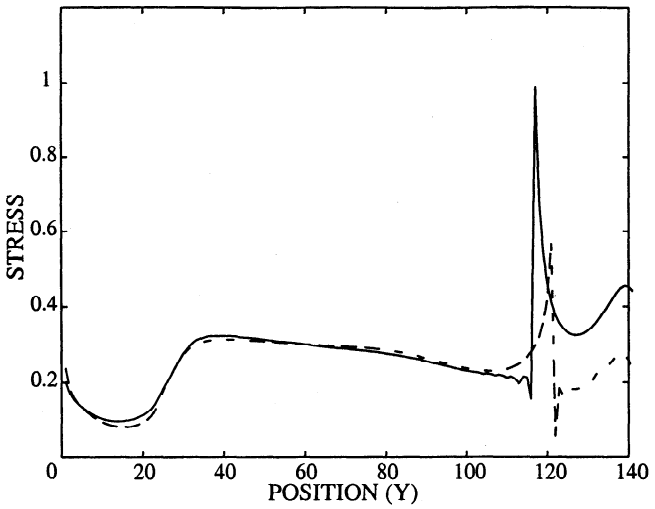

Figure 10. Cross section of the stress fields illustrated in Figure 9. The solid curve corresponds to the coarser grid ($dx = 1$) and the dashed curve corresponds to the finer grid ($dx = 0.5$). While the long wavelengths have nearly converged, a significant discrepancy in the quasi-singular stress peaks at the location of healing remains.

value of the τ parameter. However, the onset of stiction does not require in itself a consistent recovery of strength and thus cannot be turned into a gradual process. In that sense the onset of stick is the most nonlinear process in the problem.

Comparing the stress fields obtained at different spatial resolution in Figure 9, we see that the similarity in the long-wavelength characteristics obtained for the two different grids is fairly good, while the discrepancy is most pronounced at the quasi-singularity. In Figure 10 we superimpose a cross section of the two results which runs through the stress concentration. While, over time, the differences between the two grid resolutions in Figure 9 eventually lead to substantial differences in the rupture area and moment release in the sequence of events, the differences are negligible for a single event and remain small for a few successive events. Moreover, the properties of stress heterogeneity and complexity are invariant to the grid resolution, since the source of the stress variations is associated with the frictional healing rather than discretization.

We summarize our results on recurrent ruptures in Figure 11, where we illustrate a sequence of scatter plots for the area of slip versus the average rise time of rupture for three values of δ/τ corresponding to the three different regimes. Figure 11a illustrates the periodic regime in which all of the events are coincident after four initial transient ruptures. Figure 11b illustrates the aperiodic case. Here the large events form a more diffuse population on the graph. While they all span the system (thus have equal area), their average rise time varies, owing largely to variations in the position of the nucleation site relative to the boundaries. In this case there is also a population of smaller events in which nucleation criterion fails to produce a propagating rup-

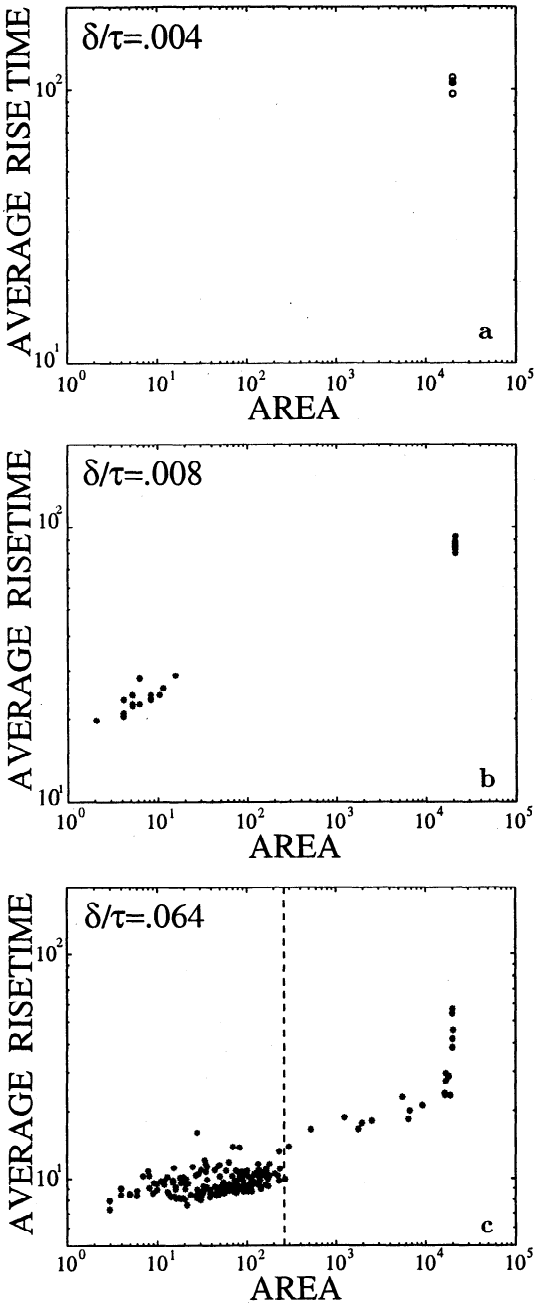

Figure 11. Total rupture area versus rise time for three different dynamical regimes, obtained for different values of δ/τ. Each dot marks an individual event in a simulation of repeated ruptures for (a) periodicity, (b) aperiodic systemwide events, and (c) dynamical complexity. The rupture area is the total area on the fault that slips. The average pulse duration is the duration of active slip at a point of the fault, averaged over the rupture area. In Figure 11a (low δ/τ) the first three events converge toward a stable limit cycle, after which the remaining 17 events are virtually identical and overlap on the diagram. In Figure 11c (intermediate δ/τ) the large events span the system and thus have the same rupture area. However, the average rise time differs somewhat due to variations in the dynamics. In Figure 11c (large δ/τ) the large events have variable area and rise time. Areas $< 200 - 300$ (marked with vertical dashed line) correspond to aborted nucleations, i.e., events which fail to propagate beyond the immediate perimeter of the initial rupture patch.

ture. Instead, the slip rapidly decays once it emerges from the triggering asperity. Because our nucleation criterion is only justified as a starting point for events that ultimately evolve to become much larger than the initial triggering zone, we do not view these rapidly aborted events as physically meaningful. Finally, Figure 11c illustrates the regime in which we observe dynamical complexity. In this regime, we have a broad distribution of the sizes of events of variable area and duration. As in Figure 11b, the smallest events will be sensitive to our (artificial) nucleation criterion. However, there remain several events with rupture areas ranging between roughly 20 and 19,600 dimensionless units in which the system develops well-formed, propagating, self-healing pulses which terminate before reaching the boundary.

Finally, we comment on the effects of varying the overall size and aspect ratio of the system. Reduction and expansion of the fault should lead to limiting behaviors. For example, for a fixed value of δ/τ which exhibits complexity on a larger system, reducing the system size will reduce the probability that slip pulses will encounter stress inhomogeneities which are sufficiently large to terminate the rupture, which in turn increases the likelihood of systemwide events. Indeed, we observe a crossover from dynamical complexity to aperiodic systemwide events as the fault size is reduced. However, we have not seen the onset of periodicity by reducing the fault size further. Instead, we run into the unphysical situation in which the size of the fault is close to the characteristic size associated with our nucleation criterion first. For this reason it would be preferable to study size effects by beginning with a periodic state and looking for crossovers to different regimes as the size of the fault is increased. However, the extent to which we can increase the system size is sufficiently limited by computational resources that we are unable to obtain conclusive results.

Increasing the aspect ratio of the fault can lead to a crossover from periodicity to aperiodic systemwide events to dynamical complexity. As was noted in section 3.2, reduction of the linear size of a square fault eventually leads to crack-like ruptures. In this regime, when the length L and width W of the fault are different, it is the shortest length scale (here assumed to be W) which controls the width of the rupture. Then, when L is increased for a fixed value of W, we observe a crossover to dynamical complexity.

We have performed simulations where the ratio L/W takes various values in the interval $[1, 12]$ for friction parameters $\delta = 0.5$ and $\tau = 100$. For these parameters, the square fault ($L/W = 1$) is in the periodic regime 1. Asymmetric faults exhibit aperiodic behavior(2 for $L/W = 2.2$, and dynamical complexity 3 for $L/W = 12$. Given the numerical limitations, models with $L/W = 12$ were obtained by shrinking the width down to $W = 20$ lattice units while holding the length at $L = 240$. Moment versus time is illustrated for the same total number of large events for the latter two cases in Figure 12. The moment, defined as the integral of slip for each event (in dimensionless units), was scaled in relation to the total fault area in order to compare both cases. Note here that in addition to the variability in size, as the aspect ratio is increased, we observe increasing variability in the time intervals between events, measured in terms of the loading increments associated with our nucleation criterion, and after an initial transient regime, the events systematically stop before reaching the entire fault area, at least within the time interval computed.

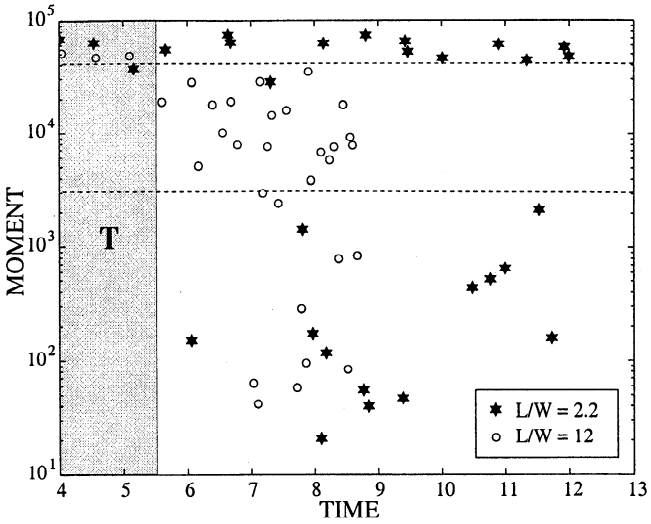

Figure 12. Moment release versus time for 30 repeated ruptures on faults with different aspect ratios. Here the moment is given by the total slip, and time is measured in terms of the cumulative increase in the load between ruptures. The stars correspond to the smaller aspect ratio $L/W = 2.2$, and the circles correspond to the larger aspect ration $L/W = 12$. For these parameters ($\delta = 2$, $\tau = 10$) the square fault with $L = 140$ exhibits periodicity. For $L/W = 2.2$ we observe aperiodic systemwide events, while for $L/W = 12$ we observe dynamical complexity, with a broad distribution of sizes of events. The shaded area marks the final stages of a transient regime where the fault is still influenced by an arbitrary imposed initial stress. The subsequent ruptures are part of a self-generated stationary regime on the fault. The two horizontal dashed lines delimit an interval containing the moment of intermediate size events, i.e., neither system-wide events nor aborted nucleations. Note that the catalog corresponding to $L/W = 2.2$ has only two events in that interval, while the catalog corresponding to $L/W = 12$ has no system-wide events after the initial transient is terminated. These simulations are carried out in a regime where the pulse length scales with the fault width W.

4. Burridge–Knopoff Model

In this section we compare the results which we have obtained for the continuum model with analogous measurements for a one-dimensional Burridge–Knopoff model [*Burridge and Knopoff*, 1967; *Carlson and Langer*, 1989a, b; *Carlson et al.*, 1991, 1994, 1996].

The dimensionless equation of motion for the BK model is given by

$$\ddot{U} = \zeta^2 \nabla^2 U - (U - Vt) - F(\dot{U}, \theta). \quad (10)$$

In the finite difference approximation the model consists of an elastically coupled chain of slider blocks, where each block is connected to a spring (analogous to the spring which drives the individual slider block in section 2) which is pulled from the opposite end at constant velocity V. The cumulative displacement $U(x,t)$ is equivalent to the slip since we work in a frame where the opposite side of the fault is stationary. Here $U(x,t)$ is a function of both the spatial grid position x and time t. The first term on the right-hand side represents the force due to compressional deformations along the fault, and the second term represents the force due to shear deformation. The final term is the frictional dissipation, given by equations (1)–(2). We retain the parameter ζ in order to explicitly account for variations in the grid spacing. Here ζ corresponds to the number of grid points a sound wave travels in unit time in the absence of dissipation. In the continuum limit $\zeta \to \infty$, and the position $s = x/\zeta$ becomes a continuous variable. For convenience we introduce a small parameter, which is an initial drop in the friction. As was shown by *Carlson et al.* [1991], this enables us to study larger system sizes in the $V \to 0^+$ limit.

Previous studies using both velocity and slip-weaking friction laws have focused primarily on regimes in which this model exhibits narrow, self-healing slip pulses and dynamical complexity qualitatively similar to the behavior we have observed in the continuum model for large values of δ/τ. Because the BK model is one dimensional, it is possible to consider orders-of-magnitude longer-fault models, over orders-of-magnitude longer times, and to load the fault at infinitesimal rates so that the full spectrum of events may be included. However, in this section we will focus on the kinds of measurements which are most analogous to those performed in the preceding section for the continuum model. Our goal is to distinguish the dynamical properties which are qualitatively similar for the BK and continuum models from those which are not as the friction parameters are varied.

Before we proceed to discuss these results, we briefly consider some fundamental contrasts between the continuum and BK models, along with strategies through which some of the more realistic features of the continuum could be represented in lower-dimensional models. Additional consequences of embedding a fault in the continuum and the effects of radiation are discussed by *Nielsen et al.* [1995].

First, typically the BK model does not explicitly account for the energy loss which is associated with the radiation of elastic waves. It will be our strategy to incorporate a viscous term in the friction ($\eta > 0$ in equation (1)) as was done previously by *Burridge and Knopoff* [1967] and *Knopoff et al.* [1992]. The amount of radiation in the continuum is approximately proportional to the slip rate, from Betti's Representation Theorem (equation (6)). Viscous terms also have the effect of introducing a short-wavelength cutoff, as discussed by *Shaw* [1994, 1997]. Because we are more interested in qualitative than quantitative comparisons here, we will make no special attempt to tune the viscous parameter.

A second important difference is the lack of long-range elastic interactions in the one-dimensional BK model, where no stress is transmitted from one point of the fault to another except through active slip of neighboring blocks. As a consequence, the stress is localized at the endpoints of the events, in contrast to the $1/\sqrt{r}$ decay which is observed for the continuum. This a priori prevents the BK model from exhibiting self-similar stress fields as observed in continuum models [*Kostrov*, 1964]. This disparity can be accounted for in part by introducing long-range couplings (see, e.g., *Chen et al.* [1991]) or considering a two-dimensional BK model [*Myers et al.*, 1996, *Langer et al.*, 1996], which has previously been seen to exhibit dynamical complexity qualitatively similar to the one-dimensional case for velocity and slip-weakening friction laws. We will not adopt either of those strategies here.

Finally, a third distinction is associated with the load, which is transmitted through leaf springs in the BK model. The spring stiffness leads to a characteristic displacement which is not present in an infinite continuum medium. However, to a rough approximation the stiffness of the BK system is analogous to the natural stiffness associated with the depth of the fault. For this reason, the results obtained for the continuum model with large aspect ratios are most analogous to the BK model.

Now we proceed to our numerical results. As in section 3.2, we first consider individual large ruptures, which nucleate at an overstressed asperity and propagate through regions of homogeneous prestress. Our initial state is generated by varying the displacements $U(x,0)$ in order to construct a central asperity, in which the prestress is slightly in excess of the friction threshold. The asperity is joined via a quadratically smooth connecting region to a large region of homogeneous prestress set somewhat below the friction threshold. This region is enclosed by energy-absorbing barriers of decreasing prestress at the edge of the system generated by quadratically increasing $U(x,0)$ corresponding to the absorbing boundary.

At time $t = 0$, slip initiates uniformly at the asperity and subsequently propagates left and right into the understressed regions, where the amplitude eventually reaches a steady state. The rupture begins to decay in the barrier regions and finally stops near the edge. At any given instant, only a small number of blocks are slipping.

Figure 13a illustrates the velocity $\dot{U}(x,t)$ as a function of position x for a specific intermediate state. In

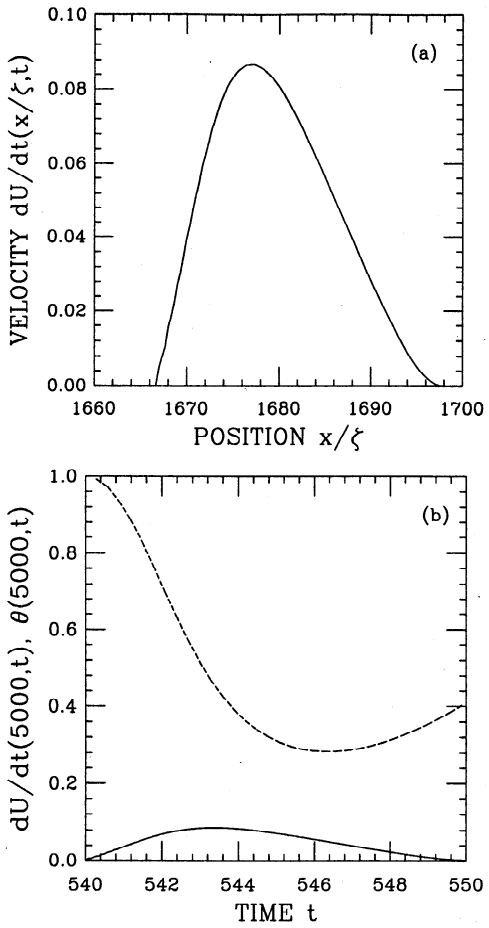

Figure 13. Properties of the narrow self-healing slip pulses in the BK model. (a) Slip velocity $\dot{U}$ as a function of the scaled position at a particular instant in time for a left propagating slip pulse. The self-healing pulse consists of roughly 100 or the 20,000 sites. (b) Slip rate (solid line) and state variable (dashed line) as a function of time at a particular site $x = 5000$. The results shown here are for $\delta = 0.2$, $\tau = 10$, $\eta = 3$, $\zeta = 20$, and system size $L = 20,000$ elements.

this particular case, the propagating slip pulse consists of roughly 100 of the 20,000 total elements. The solution corresponds to a narrow, self-healing pulse. In contrast to the continuum case, the narrow pulses we observe in the BK model are steady-state solutions. The velocity, width, and rise time approach fixed values, independent of the size of the system for systems which are sufficiently large.

In Figure 13b we plot the corresponding slip speed $\dot{U}(x,t)$ and the state variable $\theta(x,t)$ as a function of time t at a specific spatial location $x = 5000$ which is in the homogeneous region, far enough from the asperity that the pulse has achieved steady state. While we have not attempted to make an exact correspondence between the BK and continuum parameters, the scaling of the rupture width with frictional parameters for our BK solutions most closely resemble the continuum (Figure 4) when the system is overdamped ($\eta > 2$).

As is illustrated in Figure 14, the pulse width increases with decreasing δ/τ as in the continuum. In contrast, for underdamped pulses the rise time is controlled by the inertial time scale of a single slider (Figure 2a), and the pulse width depends only on δ. It is possible in the BK model to obtain crack-like slip pulses which heal in response to edge effects by decreasing the system size or increasing η. However, upon increasing the system size, we always observe a limiting pulse width, such that for systems larger than a given size, boundary effects do not play a role, and the slip pulse is self-healing.

Finally, we consider the properties of recurrent ruptures. For the BK model, we drive the system at an infinitesimal rate (as opposed to invoking an artificial nucleation criterion as we did for the continuum). As has been observed in prior studies using velocity- and slip-weakening friction laws [*Carlson and Langer*, 1989a, b; *Carlson et al.*, 1991, 1994, 1996], for the spectrum of parameters we have considered, we obtain broad distributions of sizes of events, where the distributions of the largest events cut off at a characteristic size which is independent of the system size.

In Figure 15 we plot the displacement as a function of position after the initial transient period has passed and the system has reached a statistically steady state. A new curve is drawn after each moderate or large event. In Figure 15a we illustrate results for $\delta = 0.2$ and $\tau = 10$. Clearly, the large events involve irregular displacements. The recurrence intervals are broadly dis-

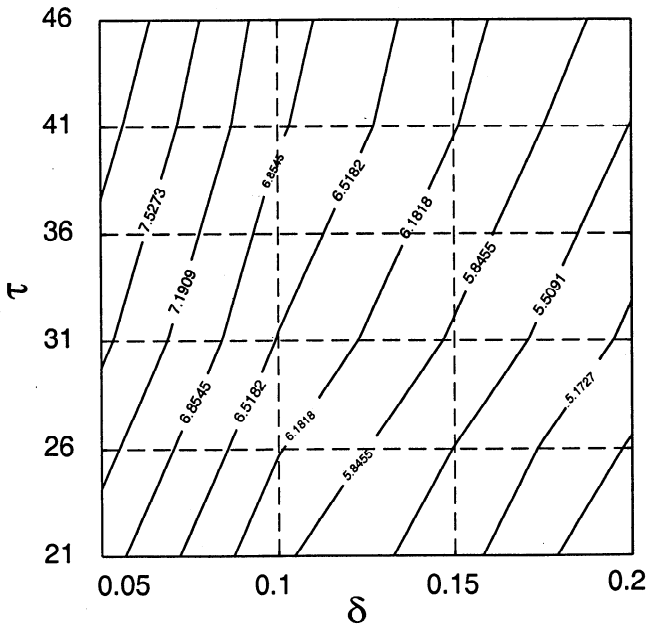

Figure 14. Contours of constant steady state pulse width $\Delta x/\zeta$ are shown as a function of the friction parameters δ and τ for the overdamped case. The results shown for $\delta = 0.2$, $\tau = 10$, and $\eta = 3$, $\zeta = 10$ are in qualitative agreement with the corresponding results in Figure 7 for the continuum model.

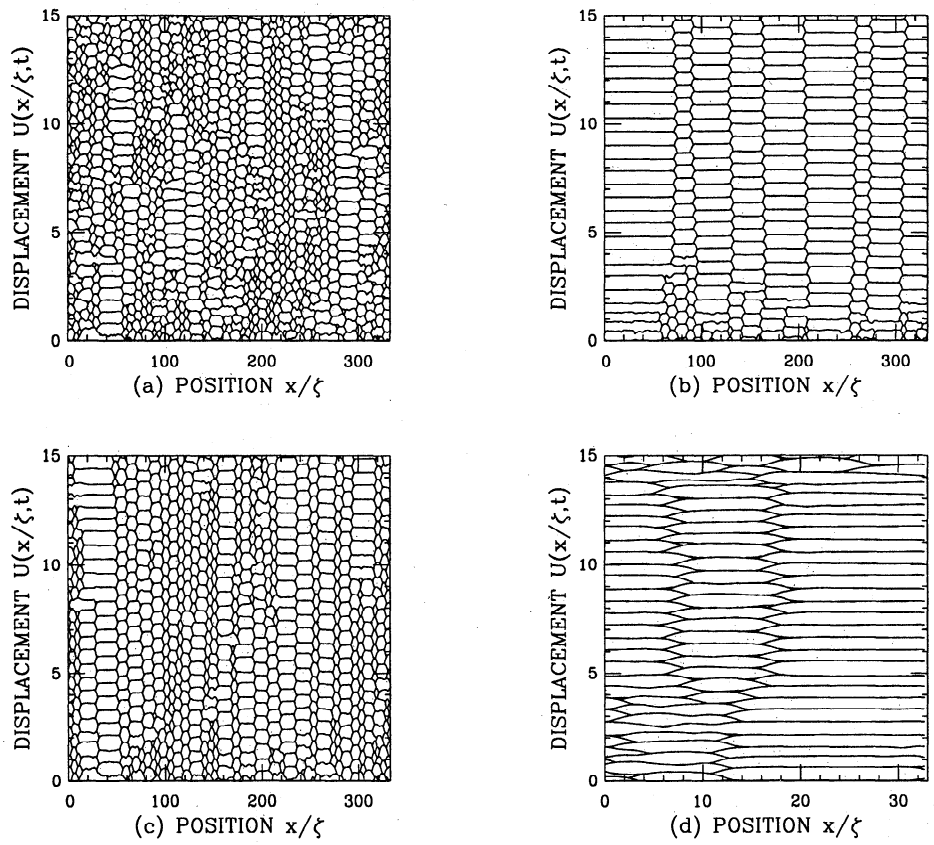

Figure 15. Complexity in the Burridge–Knopoff model. Here we plot the cumulative displacement as a function of the scaled position. A new curve is drawn after each event, and the area between consecutive curves represents the moment of the event. Results are shown for (a) $\delta = 0.2$, $\tau = 10$, and $L = 1000$; (b) $\delta = 0.2$, $\tau = 20$, and $L = 1000$; (c) $\delta = 0.1$, $\tau = 10$, and $L = 1000$; and (d) $\delta = 0.2$, $\tau = 10$, and $L = 100$. For all four graphs, $\beta = 3$ and $\zeta = 3$. Large event complexity decreases with decreasing δ, increasing τ, and decreasing L.

tributed, and the pattern of events is irregular both in space and time. In comparison, increasing the value of τ leads to much more regular behavior, as is illustrated in Figure15b. In this case, although the configuration does evolve slowly with time, for a sustained period a given location along the fault exhibits very regular and repeatable events (for a small number of events, comparable to the number we can simulate for the continuum, the system appears periodic). As is illustrated in Figure 15c in comparison to Figure 15a, decreasing the value of δ leads to an increase in the characteristic size of the largest events, which also leads to somewhat more regular behavior, though the results are not as striking as in Figure 15b. In Figures 15a-15c the system size L is taken to be larger than the characteristic size of the largest events, so that no event spans the system. In Figure 15d we show how reducing the system size also increases the regularity of recurrence. In this case, most of the large events span the system. Results are shown for periodic boundary conditions. For the BK model, the behavior of models with periodic, absorbing, and free boundary conditions is essentially identical for system sizes sufficiently large.

Our primary conclusion is that changes in the friction parameters and system size have a qualitatively similar effect on the complexity of the BK model and the continuum system. That is, larger values of τ, smaller values of δ, and reduction of the system size lead to more regularity in the dynamics. However, unlike our continuum simulations, in the BK model for a given set of friction parameters we have always been able to find system sizes which are large enough to generate dynamical complexity. The clear exception to this arises in the case where the steady state friction is velocity strengthening (i.e., $\eta > \tau/\delta$), as was pointed out in the context of a different friction law by *Shaw* [1997]. Because computational resources limit the range of system sizes we can consider for the continuum, it is impossible to conclude whether complexity would ultimately arise in larger systems in the continuum case.

5. Conclusions

We have investigated the rate and state friction law introduced in section 2 in the context of a three dimensional continuum model of faulting and a BK model. In

the continuum, we observe regimes consisting of crack-like ruptures which heal in response to edge effects, as well as narrow, self-healing pulses, which are independent of boundary conditions. For repeated ruptures, the crack-like ruptures coincide with periodic or quasi-periodic large events that span the system. The onset of dynamical complexity coincides with the crossover to self-healing. Self-healing introduces strong heterogeneities in the stress field which typically act as initiation or termination locations for subsequent ruptures. It is in this regime that we begin to encounter problems with numerical resolution of sharp features in the stress configurations. However, long-wavelength properties are well resolved, and the general behavior is qualitatively insensitive to grid effects.

The ratio δ/τ, scaled by the rate $\mu/(\Delta\sigma\,\tau)$, sets the crossover between different dynamical regimes. δ/τ is the characteristic velocity associated with the friction and $\Delta\sigma\beta/\mu$ is the characteristic slip rate associated with an estimated stress drop $\Delta\sigma$ in a medium of stiffness μ and wave speed β. We observe crack-like solutions for small values of δ/τ and narrow, self-healing pulses for large values.

For recurrent ruptures, the average value of $\Delta\sigma$ is determined self-consistently for a given δ/τ. That is, although we select the average prestress (and thus $\Delta\sigma$) of the initial state, after a transient period has passed, the qualitative dynamics are insensitive to the initial setting. A more detailed study of the role of a local and time-dependent δ/τ in determining variable patterns and recurrence intervals in the regime where we observe dynamical complexity is an interesting topic for future work.

The system size and aspect ratio of the fault play a role in determining the crossover. Self-healing pulses and dynamical complexity are favored for larger systems and larger aspect ratios. Computationally, it is much more straightforward to make definite statements in the case of variable aspect ratios, where the rupture width saturates at a size determined by the shortest linear dimension of the fault. We observe crossovers from periodicity, to aperiodic systemwide events, to dynamical complexity as the aspect ratio is increased by holding the length of the fault constant and decreasing the width.

For the square fault we observe a crossover from dynamical complexity to aperiodic systemwide events as the fault size is reduced. However, upon further reduction of the fault size, we run into an unphysical limit where the system size is comparable to the size of the asperity before reaching a periodic state. In principle, it would be preferable to study finite size effects starting with a system of fixed size in the periodic regime and then systematically increasing the system size to look for crossovers. However, computational limitations place sufficiently severe restrictions on the range of sizes we can consider that we cannot make definite conclusions regarding whether it is possible to observe the full range of behaviors as a function only of system size.

This issue gets to the heart of one of the primary distinctions between the continuum model and lower-dimensional representations such as the BK model. In an infinite continuous medium, expanding Kostrov cracks are self-similar solutions [*Kostrov*, 1964]. That is, when the times, displacements, and spatial coordinates are appropriately rescaled, the solution collapses onto a unique function. In terms of the original variables, this implies that the character of the solution scales with system size. For Kostrov cracks, there is no crossover from one dynamical regime to another as a function of the system size. However, while the intermediate portions of our ruptures are Kostrov-like, our rate and state law introduces important distinctions at the initial and final stages of slip which can lead to strong stress heterogeneities induced by rapid healing.

A question which is beyond the scope of present-day computers to answer conclusively is whether all rate-weakening frictional parameters would eventually lead to self-healing and dynamical complexity for systems which are sufficiently large. On one hand, a larger system size offers more dynamical modes and more opportunity for emerging stress heterogeneity. This key feature leads to our observation of a crossover from aperiodic systemwide events to dynamical complexity. Alternatively, like Kostrov cracks the ruptures we obtain in our continuum simulations exhibit some features suggestive of self-similarity, exhibiting increasing average slip with increasing system size. For the system sizes we can consider, this occurs both for crack-like solutions and self-healing pulses. If self-similarity dominates the periodic regime, increasing the system size on a square fault may only lead to larger-scale versions of the same solutions.

When we increase the aspect ratio of the fault, we cross over to a regime in which the rupture width saturates at the fault width as it propagates along the length of the fault. In this case it is geometry, rather than friction, which sets the length scale for the pulse. This behavior is most analogous to that of the BK model, which generically exhibits narrow self-healing pulses which evolve to a steady state solution as they propagate through a homogeneous stress field for system sizes which are sufficiently large. Basic properties, such as the dependence of the rupture width on the friction parameters, can be made qualitatively similar in the BK model and the continuum when a viscosity is added to the friction law for the BK model to compensate for the lack of radiation. In addition, while the BK model much more generically exhibits dynamical complexity, it is difficult to determine whether the lack of complexity in the continuum is an intrinsic property or whether it is associated with the limited range of system sizes and time scales that can be probed numerically. We do observe that as the friction parameters and

length are varied, in the dynamically complex regime, variations in the degree of irregularity of recurrent ruptures are qualitatively similar for the BK model and the continuum case.

The computational limitations associated with the continuum model restrict our ability to go beyond qualitative comparisons between the continuum and BK studies for issues which are as broad as dynamical complexity. Observations of qualitative similarities are useful because there are many questions which can be explored in depth in the BK model which we would have no hope of probing in the continuum. The similarities and differences we have observed so far also lead to a new set of more specific questions related to obtaining the best agreement between the dynamics of individual ruptures in the two cases and a more precise characterization of the nature of the crossovers between different regimes. This represents a necessary step in an integrative approach to earthquake modeling in which results obtained from more detailed models are incorporated as approximations in simplified representations. Such an approach may provide a means for broader exploration of the wide range of scales associated with seismic phenomena given the computational tradeoffs between the time and length scales considered in simulations versus model and algorithmic accuracy.

Acknowledgments. S.N. acknowledges the support of the Material Research Laboratory and the Institute for Crustal Studies, University of Southern California, Santa Barbara. This is ICS publication 0352-97EQ. This work was supported by the MRSEC Program of the National Science Foundation under award DMR96-32716, by the David and Lucile Packard Foundation and by NSF grants DMR-9212396 and DMR-9813752. The computations in this study were carried out on the SGI Origin 2000 at UCSB (NSF grant CDA96-01954).

References

Aki, K., and P. Richards, *Quantitative Seismology*, vol. *II*, W. H. Freeman, New York, 1980.

Andrews, D. J., Rupture propagation with finite stress in antiplane strain, *J. Geophys. Res.*, *81*, 3575–3582, 1976.

Beeler, N. M., and T. E. Tullis, Self-healing slip pulses in dynamic ruptures models due to velocity-dependent strength, *Bull. Seismol. Soc. Am.*, *86*, 1130–1148, 1996.

Ben-Zion, Y., and J. Rice, Earthquake failure sequences along a cellular fault zone in a three-dimensional elastic solid containing asperity and nonasperity regions, *J. Geophys. Res.*, *98*, 14,109–14,131, 1993.

Ben-Zion, Y., and J. R. Rice, Dynamic simulations of slip in a smooth fault in an elastic solid, *J. Geophys. Res.*, *102*, 17,771–17,784, 1997.

Beroza, G., and T. Mikumo, Short slip duration in dynamic rupture in the presence of heterogeneous fault properties *J. Geophys. Res.*, *101*, 22,449–22,460, 1996.

Brune, J. N., Tectonic stress and the spectra of seismic shear waves from earthquakes *J. Geophys. Res.*, *75*, 4997-5009, 1970.

Burridge, R., and L. Knopoff, Model and theoretical seismicity, *Bull. Seismol. Soc. Am.*, *57*, 341–371, 1967.

Burridge, R., and R. Moon, Slipping on a frictional fault plane in three dimensions: A numerical simulation of a scalar analogue, *Geophys. J. R. Astron. Soc.*, *67*(2), 325–342, 1981.

Carlson, J. M., and A. A. Batista, Constitutive relation for the friction between lubricated surfaces, *Phys. Rev. E*, *53*, 4153–4165, 1996.

Carlson, J. M., and J. S. Langer, Properties of earthquakes generated by fault dynamics, *Phys. Rev. Lett.*, *62*, 2632–2635, 1989a.

Carlson, J. M., and J. S. Langer, Mechanical model of an earthquake fault, *Phys. Rev. A*, *40*, 6470–6484, 1989b.

Carlson, J. M., J. S. Langer, B. E. Shaw, and C. Tang, Intrinsic properties of a Burridge-Knopoff model of an earthquake fault, *Phys. Rev. A*, *44*, 884–897, 1991.

Carlson, J. M., J. Langer, and B. E. Shaw, Dynamics of earthquake faults, *Rev. Mod. Phys.*, *66*, 657–670, 1994.

Carlson, J. M., S. P. Pepke, and V. G. Kossobokov, Prediction studies of earthquake fault models and applications to seismic catalogs, edited by J. B. Rundle, D. L. Turcotte, and M. W. Klein, in *Reduction and Predictability of Natural Disasters*, pp. 273–291, Addison-Wesley-Longman, Reading, Mass., 1996.

Chen, K., P. Bak, and S. P. Obukhov, Self-organized criticality in a crack-propagation model of earthquakes, *Phys. Rev. A*, *43*, 625–630, 1991.

Christensen, K., and Z. Olami, Variaton of the Gutenberg-Richter *b* values and nontrivial temporal correlations in a spring-block model for earthquakes, *J. Geophys. Res.*, *97*, 8729–8735, 1992.

Cochard, A., and R. Madariaga, Dynamic faulting under rate-dependent friction, *Pure Appl. Geophys.*, *142*, 419–445, 1994.

Cochard, A., and R. Madariaga, Complexity of seismicity due to highly rate-dependent friction, *J. Geophys. Res.*, *101*, 25,321–25,336, 1996.

Cochard, A., and J. Rice, Mode of rupture, self-healing pulse versus enlarging shear crack, for a velocity weakening fault in a 3d solid (abstract), *Eos Trans. AGU*, *78*(46), Fall Meet. Suppl., F472, 1997.

Dahlen, F. A., On the ratio of *P*-wave to *S*-wave corner frequencies for shallow earthquake sources, *Bull. Seismol. Soc. Am.*, *64*, 1159–1180, 1974.

Day, S. M., Three-dimensional finite difference simulation of fault dynamics: Rectangular faults with fixed rupture velocity, *Bull. Seismol. Soc. Am.*, *72*, 705–727, 1982.

Day, S. M., G. Yu, and D. J. Wald, Dynamic stress changes during earthquake rupture *Bull. Seismol. Soc. Am.*, *88*, 512-522, 1998.

Dieterich, J. H., Time-dependent friction and the mechanics of stick-slip, *Pure Appl. Geophys.*, *116*, 790–806, 1978.

Dieterich, J. H., Modeling of rock friction, 2, Simulation of preseismic slip, *J. Geophys. Res.*, *84*, 2169–2175, 1979.

Dieterich, J. H., A constitutive law for rate of earthquake production and its application to earthquake clustering, *J. Geophys. Res.*, *99*, 2601–2618, 1994.

Dieterich, J. H., and B. Kilgore, Direct observation of frictional contacts: new insights for state-dependent properties, *Pure Appl. Geophys.*, *143*, 283–302, 1994.

Guatteri, M., and P. Spudich, The effect of absolute stress on dynamic rupture, *Bull. Seismol. Soc. Am.*, *88*, 777–789, 1998.

Harris, R. A., and S. M. Day, Dynamics of fault interaction: Parallel strike-slip faults, *J. Geophys. Res.*, *98*

Heaton, T. H., Evidence for and implications of self-healing pulses of slip in earthquake rupture, *Phys. Earth Planet. Inter.*, *64*, 1–20, 1990.

Ide, S., and M. Takeo, Determination of constitutive re-

lations of fault slip based on seismic wave analysis, *J. Geophys. Res.*, *102*, 27379–27391, 1997.

Knopoff, L., J.A. Landoni, and M. Abinante, Dynamical model of an earthquake fault with localisation, *Phys. Rev. A*, *46*, 7445-7449, 1992.

Kostrov, B. V., Self-similar problems of propagation of shear cracks, *J. Appl. Math. Mech.*, *28*, 1077–1087, 1964.

Lachenbruch, A. H., Frictional heating, fluid pressure, and the resistance to fault motion, *J. Geophys. Res.*, *85*, 6097–6112, 1980.

Langer, J. S., J. M. Carlson, C. M. Myers, and B. E. Shaw, Slip complexity in dynamic models of earthquake faults, *Proc. Natl. Acad. Sci.*, U.S.A., *93*, 3825–3829, 1996.

Leung, K., J. Anderson, and D. Sornette, Self-organized criticality in stick-slip models with periodic boundaries, *Phys. Rev. Lett.*, *80*, 1916–1919, 1998.

Madariaga, R., Dynamics of an expanding circular fault, *Bull. Seismol. Soc. Am.*, *66*, 639–666, 1976.

Madariaga, R., K. Olsen, and R. Archuleta, 3-d finite-difference simulation of a dynamic rupture (abstract), *Eos Trans. AGU*, *77*(46), Fall Meet. Suppl., F470, 1996.

Marone, C., and B. Kilgore, Scaling of the critical slip distance for seismic faulting with shear strain in fault zones, *Nature*, *362*, 618–620, 1993.

Myers, C. R., B. E. Shaw, and J. S. Langer, Slip complexity in a crustal-plane model of an earthquake fault, *Phys. Rev. Lett.*, *77*, 972–975, 1996.

Nielsen, S. B., and K. B. Olsen, A new mixed boundary condition for rupture simulation in finite differences (abstract), *Eos Trans. AGU*, *79*(45), Fall Meet. Suppl., F630, 1998.

Nielsen, S. B., L. Knopoff, and A. Tarantola, Model of earthquake recurrence: Role of elastic wave radiation, relaxation of friction and inhomogeneity, *J. Geophys. Res.*, *100*, 12,423–12,430, 1995.

Olsen, K. B., R. Madariaga, and R. J. Arculeta, Three-dimensional dynamic simulation of the 1992 landers earthquake, *Science*, *278*, 834–838, 1997.

Pepke, S. L., J. M. Carlson, and B. E. Shaw, Prediction of large events in a dynamical model of a fault, *J. Geophys. Res.*, *99*, 6769–6788, 1994.

Perrin, G. O., J. R. Rice, and G. Zheng, Self-healing slip pulse on a frictional surface, *J. Mech. Phys. Solids*, *43*, 1461–1495, 1995.

Rice, J. R., Spatio-temporal complexity of slip on a fault, *J. Geophys. Res.*, *98*, 9885–9907, 1993.

Rice, J. R., and A. L. Ruina, Stability of steady frictional slipping, *J. Appl. Mech.*, *50*, 343–349, 1983.

Rice, J. R., and Y. Ben-Zion, Slip complexity in earthquake fault models, *Proc. Natl. Acad. Sci.*, U.S.A., *93*, 3811-3818, 1996.

Rice, J. R., Y. Ben-Zion, and K.-S. Kim, Three-dimensional perturbation solution for a dynamic planar crack moving unsteadily in a model elastic solid, *J. Mech. Phys. Solids*, *42*, 813–843, 1994.

Rice, J. R., and S. T. Tse, Dynamic motion of a single degree of freedom system following a rate and state dependent friction law, *J. Geophys. Res.*, *91*, 521–530, 1986.

Ruina, A., Slip instability and state variable friction laws, *J. Geophys. Res.*, *88*, 10,359–10,370, 1983.

Rundle, J., W. Klein, S. Gross, and D. Turcotte, Boltzmann fluctuations in numerical simulations of nonequilibrium lattice threshold systems, *Phys. Rev. Lett.*, *75*, 1658–1661, 1995.

Shaw, B. E., Complexity in a spatially uniform continuum fault model, *Geophys. Res. Lett.*, *21*, 1983–1986, 1994.

Shaw, B. E., Frictional weakening and slip complexity in earthquake faults, *J. Geophys. Res.*, *100*, 18,239–18,251, 1995.

Shaw, B. E., Model quakes in the two-dimensional wave equation, *J. Geophys. Res.*, *102*, 27,367–27,377, 1997.

Sibson, R., Fault zone models, heat flow, and the depth distribution of earthquakes in the continental crust of the United States, *Bull. Seismol. Soc. Am.*, *72*, 151–163, 1982.

Spudich, P., Use of fault striations and dislocation models to infer tectonic shear stress during the 1995 Hyogo-ken Nanbu (Kobe), Japan, earthquake, *Bull. Seismol. Soc. Am.*, *88*, 413–427, 1998.

Thompson, P. A., and M. O. Robbins, Origin of stick-slip motion in boundary lubrication, *Science*, *250*, 792–794, 1990.

Tullis, T. E., and J. Weeks, Constitutive behavior and stability of frictional sliding of granite, *Pure Appl. Geophys.*, *124*, 383–414, 1986.

Zheng, G. and J. Rice, Conditions under which velocity weakening friction allows a self-healing versus a cracklike mode of rupture, *Bull. Seismol. Soc. Am.*, *88*, 1466–1483, 1998.

J. M. Carlson, Department of Physics, University of California, Santa Barbara, CA 93106.

S. Nielsen and K. B. Olsen, Institute of Crustal Studies, University of California, Santa Barbara, CA 93106-1100. (snielsen@quake.ucsb.edu; kbolsen@quake.ucsb.edu)

(Received February 16, 1999; revised August 23, 1999; accepted September 30, 1999.)